Backward optical parametric oscillator threshold and linewidth studies

Antoine Godard, Marie Guionie, Jean-Baptiste Dherbecourt, Jean-Michel Melkonian, Myriam Raybaut

Backward optical parametric oscillator threshold and linewidth studies

ANTOINE GODARD*, MARIE GUIONIE, JEAN-BAPTISTE DHERBECOURT, JEAN-MICHEL MELKONIAN, AND MYRIAM RAYBAUT

DPHY, ONERA, Université Paris-Saclay, F-91123 Palaiseau, France
**antoine.godard@onera.fr*

Abstract: We carry out the theoretical investigation of the backward interaction optical parametric oscillator (OPO), in which one of the generated waves is counterpropagating with respect to the pump. We derive simple, self-consistent analytical formulas for the continuous-wave and pulsed regimes. While consistent with previous works on continuous-wave regime, our study enables to extend the analysis to the pulsed regime. In particular, we derive simple expressions of the oscillation build-up time, pulsed threshold and efficiency, for the first time to our knowledge. We also investigate the peculiar spectral features of the backward OPO when pumped with a narrow-linewidth pulsed radiation, in particular the absence of tolerance to phase mismatch and the natural ability to emit two waves with a Fourier-transform limited spectrum. Comparison with the convention forward OPO are also carried out to emphasize the unique properties of the backward OPO.

1. Introduction

Initially proposed by Harris in 1966 [1], the backward-wave optical parametric oscillator (BWOPO) is based on three-wave second-order nonlinear interaction in a nonlinear medium where one generated wave, referred as the backward wave, propagates in the opposite direction of the incident pump wave and the other generated wave, referred as the forward wave. In contrast to conventional optical parametric oscillators (OPOs) based on three co-propagating waves where an external feedback has to be provided to the nonlinear medium by an optical cavity, resonant at one or the two generated waves, oscillation in a BWOPO can occur thanks to the distributed feedback due to the presence of two counter-propagating parametric waves. Thus, for its operation, the BWOPO does not require to adjust and maintain any fine alignment of cavity mirrors, making the device very simple and reliable.

Despite this striking attractive feature, it took 40 years before its experimental demonstration by Canalias and Pasiskevicius [2]. This long time gap was due to the fact that quasi-phase matching material with sub-micrometer poling period had first to be developed since conventional phase matching would require an extraordinary large birefringence. In [2], the authors also validated the unique spectral properties of the light emitted by the BWOPO, in which the spectral bandwidth of the pump wave is basically transferred to the forward wave while the backward wave exhibits a narrow spectral linewidth. These spectral properties have then been extensively investigated through experimental and numerical studies in pulsed regime and exploited to carry out coherent phase transfer from the pump wave to the signal wave [3–6].

Regarding theoretical work, general plane-wave solutions to backward three-wave mixing in the continuous-wave (CW) regime, involving Jacobi elliptic functions, were derived by Meadors in 1969 [7]. Other theoretical studies devoted to the CW BWOPO were then published [8–10]. In particular, [10] contains convenient analytical expressions to determine the CW BWOPO conversion efficiency and oscillation threshold.

Due its high CW oscillation threshold intensity, typically of 50–100 MW/cm^2, the BWOPO has only been operated in the pulsed regime so far. In this context, a theoretical analysis of the

BWOPO threshold and efficiency in the pulsed regime is worth investigating. In particular, even through most of previous reported works involved pump pulses in the 10's to 100's picoseconds duration, the BWOPO is also very promising for operation with longer nanosecond pulses [11], where its unique spectral properties are promising for applications such as lidar remote gas sensing.

Depending on the pulse duration, the pulsed threshold can be significantly higher than the CW threshold. To guide BWOPO design, it would thus be valuable to derive a BWOPO analog of the Brosnan–Byer expression of the pulsed OPO threshold [12]. A first step in this direction was taken in [13], but it was limited to the numerical investigation of the pulsed threshold as a function of the pump pulse duration and the derivation of an analytical expression of the pulsed threshold was not reported.

In this paper, we carry out the theoretical investigation of the BWOPO by extending the approach we previously applied to conventional OPOs [14–17]. Exactly taking into account the nonlinear interactions between the waves in the nonlinear crystal, we derive universal expressions for the BWOPO in CW and pulsed regimes which enables to carry out convenient comparisons with the usual singly resonant OPO (SROPO). One of the main outcomes is the derivation of the analytical expressions of the BWOPO pulsed threshold and build-up time as well as the optimal pulse duration to minimize the threshold energy. We also provide an approximate expression of the pulsed conversion efficiency which could also be helpful for the design of a BWOPO. We finally carry out numerical simulation of the BWOPO by finite-difference time-domain (FDTD) modeling to assess the validity of our analytical expressions and further emphasize some distinctive spectral properties of the BWOPO compared to the conventional pulsed OPO.

This paper is organized as follows. Section 2 presents the analysis of the threshold and the efficiency of the pulsed BWOPO. First, the coupled-wave equations and main assumptions are presented. Secondly, we derive the exact solutions to the equations in the CW regime using Jacobi elliptic functions. We recover the expressions previously derived in the literature and compare the characteristics of the BWOPO with the conventional SROPO. In particular, we determine the mirror reflectivity to have a SROPO with the same oscillation threshold as a mirrorless BWOPO based on an equivalent nonlinear medium. Then, we derive simple expressions to evaluate the pulsed oscillation threshold and efficiency, which are reported here for the first time to our knowledge. Section 3 is devoted to the investigation of the spectral properties of the BWOPO. First, we analyse particular phase-matching acceptance which is much narrower than for forward parametric interaction. Secondly, we investigate the parametric amplification bandwidth. In particular, we show that perfect phase-matching is required to be able to reach the BWOPO threshold. Thirdly, numerical calculations are carried out to validate the analytical results and to compare the spectral properties of the BWOPO with the conventional SROPO. The calculation confirms the ability of the BWOPO to naturally deliver single frequency radiation with a Fourier-transform linewidth. The final section summarizes the conclusions.

2. Backward OPO threshold and efficiency

2.1. Coupled-wave equations

The geometry of the studied BWOPO is shown in Fig. 1. We consider a second-order nonlinear material of length L containing a quasi-phase-matching grating to enable efficient interaction with a backward propagating wave. For the theoretical analysis, we start with the nonlinear three-wave mixing coupled equations in the slowly-varying envelope approximation which reduce

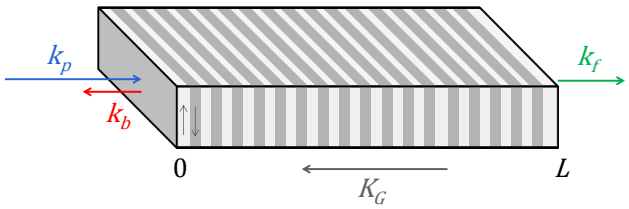

Fig. 1. Schematic of the BWOPO based on a periodically domain-inverted ferroelectric crystal.

in the plane-wave limit to [4, 18]

$$\frac{\partial A_b}{\partial z} - \frac{1}{v_{gb}}\frac{\partial A_b}{\partial t} = -i\kappa A_p A_f^* \exp\left(i\Delta k z\right), \tag{1a}$$

$$\frac{\partial A_f}{\partial z} + \frac{1}{v_{gf}}\frac{\partial A_f}{\partial t} = i\kappa A_p A_b^* \exp\left(i\Delta k z\right), \tag{1b}$$

$$\frac{\partial A_p}{\partial z} + \frac{1}{v_{gp}}\frac{\partial A_p}{\partial t} = i\kappa A_b A_f \exp\left(-i\Delta k z\right), \tag{1c}$$

with v_{gj} the group velocity of wave j, where $j = b$, f, and p corresponds respectively to the backward, forward, and pump wave, κ the nonlinear coupling coefficient

$$\kappa = \frac{d_{\text{eff}}}{c}\sqrt{\frac{\omega_b \omega_f \omega_p}{n_b n_f n_p}}, \tag{2}$$

with d_{eff} the effective nonlinear coefficient. A_b, A_f, and A_p are the complex amplitudes related to the real electric fields as follows:

$$E_b\left(z,t\right) = \frac{1}{2}\sqrt{\frac{\omega_b}{n_b}} A_b\left(z,t\right)\exp\left[i\left(-k_b z - \omega_b t\right)\right] + c.c., \tag{3a}$$

$$E_{p,f}\left(z,t\right) = \frac{1}{2}\sqrt{\frac{\omega_{p,f}}{n_{p,f}}} A_{p,f}\left(z,t\right)\exp\left[i\left(k_{p,f} z - \omega_{p,f} t\right)\right] + c.c., \tag{3b}$$

where n_j, ω_j, and k_j are respectively the refractive index, angular frequency and wavevector of wave j, and Δk is the phase mismatch

$$\Delta k = k_p - k_f + k_b - K_G, \tag{4}$$

with K_G the quasi-phase matching wavevector. The analysis is limited to plane waves in order to derive simple formulas. The investigation of finite beam effects which would require a more elaborate model is beyond the scope of this paper. The model could nonetheless be straightforwardly extended to waveguide structures by using mode propagation constants instead of wavevectors, introducing mode overlap integrals, and, if necessary, adding waveguide losses.

For simplicity's sake, we consider that the magnitude of the group velocity is the same for the three waves. However, since the backward wave propagates in the opposite direction, its group velocity has an opposite sign compared to the group velocity of the forward and pump waves. As a consequence, the relative group velocity difference is very large given that it is equal to $2v_g$, which is dominant compared to other chromatic dispersion effects. Thereby, coupled equations

(1a)-(1c) become

$$\frac{\partial A_b}{\partial z} - \frac{1}{v_g}\frac{\partial A_b}{\partial t} = -i\kappa A_p A_f^*, \tag{5a}$$

$$\frac{\partial A_f}{\partial z} + \frac{1}{v_g}\frac{\partial A_f}{\partial t} = i\kappa A_p A_b^*, \tag{5b}$$

$$\frac{\partial A_p}{\partial z} + \frac{1}{v_g}\frac{\partial A_p}{\partial t} = i\kappa A_b A_f, \tag{5c}$$

where perfect quasi-phase matching is also assumed to investigate the BWOPO. As shown in Section 3.2, this is actually a necessary condition for parametric oscillation.

2.2. Continuous-wave regime

In CW regime, one can discard time dependence and the related partial derivative. The system (5a)–(5c) thus simplifies into

$$\frac{\mathrm{d}A_b}{\mathrm{d}z} = -i\kappa A_p A_f^*, \tag{6a}$$

$$\frac{\mathrm{d}A_f}{\mathrm{d}z} = i\kappa A_p A_b^*, \tag{6b}$$

$$\frac{\mathrm{d}A_p}{\mathrm{d}z} = i\kappa A_b A_f, \tag{6c}$$

To solve the above system, we decompose the complex amplitudes as follows

$$A_j(z) = u_j(z)\exp\left[\varphi_j(z)\right], \tag{7}$$

where amplitude $u_j(z)$ and phase $\varphi_j(z)$ are both real-valued functions. For the BWOPO, we consider that there is no incident forward and backward waves, leading to the following boundary conditions:

$$u_f(0) = u_b(L) = 0, \tag{8}$$

and we assume that the relative phase $\Delta\varphi = \varphi_p - \varphi_b - \varphi_f$ has reached the steady-state value which maximizes the coupling between the three waves and thus satisfies $\cos[\Delta\varphi(z)] = 1$. Moreover, we take pump depletion into account by a change of sign in $u_p(z)$ rather than a step of π in $\Delta\varphi(z)$. With this additional assumption, we can know consider the following system which only involves real functions and parameters:

$$\frac{\mathrm{d}u_b}{\mathrm{d}z} = -\kappa u_p u_f, \tag{9a}$$

$$\frac{\mathrm{d}u_f}{\mathrm{d}z} = \kappa u_p u_b, \tag{9b}$$

$$\frac{\mathrm{d}u_p}{\mathrm{d}z} = -\kappa u_b u_f, \tag{9c}$$

From Eqs. (9a)–(9c), the "constants of motion" are found to be

$$u_p^2(z) + u_f^2(z) = u_{p0}^2, \tag{10a}$$

$$u_p^2(z) - u_b^2(z) = u_{p0}^2 - u_{\mathrm{out}}^2, \tag{10b}$$

$$u_f^2(z) + u_b^2(z) = u_{\mathrm{out}}^2, \tag{10c}$$

where we use the compact notations: $u_p(0) = u_{p0}$, $u_b(0) = u_f(L) = u_{\text{out}}$. These constant of motion are determined by the boundary conditions. Equation (9b) describing the evolution of the forward wave can then be rewritten as follows

$$\frac{\mathrm{d}u_f}{\mathrm{d}z} = \kappa\sqrt{\left(u_{p0}^2 - u_f^2\right)\left(u_{\text{out}}^2 - u_f^2\right)}, \tag{11}$$

which may be formally integrated as

$$\kappa z = \int_0^{u_f(z)} \frac{\mathrm{d}u_f}{\sqrt{\left(u_{p0}^2 - u_f^2\right)\left(u_{\text{out}}^2 - u_f^2\right)}}, \tag{12}$$

This latter expression has a solution in terms of Jacobi functions:

$$u_f\,(z) = u_{\text{out}}\,\mathrm{sn}\left(\kappa\, z\, u_{p0}\middle|\frac{u_{\text{out}}^2}{u_{p0}^2}\right), \tag{13}$$

where the Jacobi inverse function sn is defined by [19]

$$\int_0^x \frac{\mathrm{d}t}{\sqrt{\left(a^2 - t^2\right)\left(b^2 - t^2\right)}} = \frac{1}{a}\mathrm{sn}^{-1}\left(\frac{x}{b}\middle|\frac{b^2}{a^2}\right). \tag{14}$$

The pump and backward waves spatial evolution can then be derived by use of (10a) and (10a):

$$u_p\,(z) = u_{p0}\,\mathrm{dn}\left(\kappa\, z\, u_{p0}\middle|\frac{u_{\text{out}}^2}{u_{p0}^2}\right), \tag{15}$$

and

$$u_b\,(z) = u_{\text{out}}\,\mathrm{cn}\left(\kappa\, z\, u_{p0}\middle|\frac{u_{\text{out}}^2}{u_{p0}^2}\right), \tag{16}$$

where we use the relations between the squares of the Jacobi functions: $\mathrm{dn}^2(x|m) = 1 - m\,\mathrm{sn}^2(x|m)$ and $\mathrm{cn}^2(x|m) = 1 - \mathrm{sn}^2(x|m)$

Setting $z = L$ in (13), one obtains the implicit equation for BWOPO CW oscillation

$$\mathrm{sn}\left(\kappa\, L\, u_{p0}\middle|\frac{u_{\text{out}}^2}{u_{p0}^2}\right) = 1. \tag{17}$$

This expression is equivalent to the one derived by Meadors [7]. The CW oscillation threshold, $u_{\text{th}}^{\text{CW}}$, can then be easily derived using the approximation $\mathrm{sn}(x|m) \approx \sin(x)$ when $m \to 0$:

$$u_{\text{th}}^{\text{CW}} = \frac{\pi}{2\kappa L}. \tag{18}$$

The above expression can be conveniently expressed in terms of intensity, $I = \epsilon_0\, c\, n\, \langle E^2\rangle = \epsilon_0\, c\, \omega\, |A|^2\, /2$ (in W/m^2), as follows:

$$I_{\text{th}}^{\text{CW}} = \frac{\epsilon_0\, c\, n_b\, n_f\, n_p\, \lambda_b\, \lambda_f}{32 d_{\text{eff}}^2\, L^2}. \tag{19}$$

The latter expression of the threshold intensity is consistent with previously reported expressions when one take the different definitions of the effective nonlinear coefficient into account [1,7,10,13]

One can introduce the photon conversion efficiency, η, defined as

$$\eta = u_{\mathrm{out}}^2 / u_{p0}^2, \tag{20}$$

and consider that

$$\left(u_{p0} \Big/ u_{\mathrm{th}}^{\mathrm{CW}} \right)^2 = I_p / I_{\mathrm{th}}^{\mathrm{CW}}. \tag{21}$$

The implicit equation for BWOPO CW oscillation (17) can then be rewritten:

$$\mathrm{sn}\left(\frac{\pi}{2} \sqrt{I_p / I_{\mathrm{th}}^{\mathrm{CW}}} \,\middle|\, \eta \right) = 1. \tag{22}$$

After some algebra, the latter equation can also be written in terms of complete elliptic integral of the first kind as follows, which is easier and faster for numerical solving and to derive approximate expressions:

$$\frac{\pi}{2} \sqrt{I_p / I_{\mathrm{th}}^{\mathrm{CW}}} = K(\eta)\,, \tag{23}$$

with

$$K(\eta) = \int_0^1 \frac{\mathrm{d}x}{\sqrt{\left(1 - x^2\right)\left(1 - \eta x^2\right)}}. \tag{24}$$

Equation (23) is similar to the one derived by Ding and Khurgin [10].

Approximate expressions can be derived for BWOPO operation close to the oscillation threshold by use of the following expansion of $K(\eta)$:

$$K(\eta) = \frac{\pi}{2} \sum_{m=1}^{\infty} \left[\frac{\left(\frac{1}{2}\right)_m}{m!} \right]^2 \eta^m, \tag{25}$$

where Pochhammer's symbol is defined as $(a)_n = a\,(a+1)\,(a+2)\ldots(a+n-1)$. Equation (25) yields the following first- and second-order approximations:

$$\eta \simeq 4 \left(\sqrt{I_p / I_{\mathrm{th}}^{\mathrm{CW}}} - 1 \right), \tag{26}$$

and

$$\eta \simeq \frac{8}{9} \left\{ \left[1 + 9 \left(\sqrt{I_p / I_{\mathrm{th}}^{\mathrm{CW}}} - 1 \right) \right]^{1/2} - 1 \right\}. \tag{27}$$

Conversely, for high conversion efficiencies ($\eta \to 1$), the following approximation may be considered:

$$K(\eta) \simeq \frac{1}{2} \ln\left(\frac{16}{1 - \eta} \right), \tag{28}$$

which yields

$$\eta \simeq 1 - 16 \exp\left(-\pi \sqrt{I_p / I_{\mathrm{th}}^{\mathrm{CW}}} \right). \tag{29}$$

As seen in Fig. 2, the first-order approximation, (26), is only valid very close to the oscillation threshold while the second-order approximation, (27), provides a reasonable agreement (better than 10 %) for $I_p < 1.4\, I_{\mathrm{th}}^{\mathrm{CW}}$. Conversely, the accuracy of asymptotic expression (29) is better

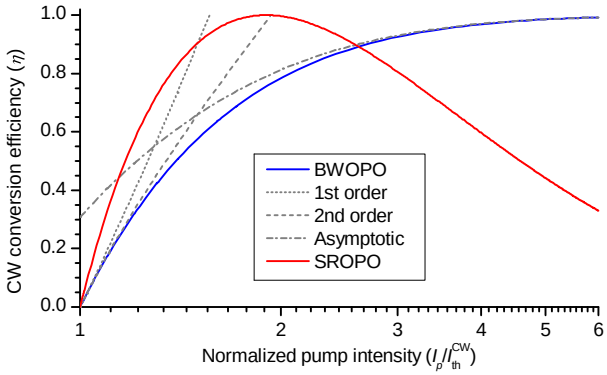

Fig. 2. CW conversion efficiency as a function of pump pump intensity normalized to the CW threshold intensity. The SROPO has a coupler reflectivity given by (31) which yields the same CW threshold intensity as the BWOPO.

than 10 % for $I_p > 1.6\, I_{\text{th}}^{\text{CW}}$. As discussed in next section, this latter approximation is actually convenient to evaluate the efficiency in pulsed regime where the involved peak intensity is often high enough.

Let us now carry out a comparison with the more conventional singly resonant OPO (SROPO) based on the forward nonlinear interaction between three co-propagating waves while the feedback is provided by an optical cavity resonant at the signal wave. Using the same formalism as the one derived here [14], the CW oscillation of the SROPO reads:

$$u_{\text{th,SROPO}}^{\text{CW}} = \frac{1}{\kappa L} \cosh^{-1}\left(\frac{1}{\sqrt{R}}\right), \tag{30}$$

where R is the output coupler reflectivity at the signal while the other loss are neglected and the mirror reflectivity is zero for the idler and the pump. Combining (18) and (30) enables to determine the coupler reflectivity, R_{SROPO}, which yields the same threshold for the BWOPO and the SROPO:

$$R_{\text{SROPO}} = \frac{1}{\cosh^2(\pi/2)} \simeq 0.16, \tag{31}$$

where we suppose that the product κL is the same for the two OPOs, i.e., we consider the same nonlinear materials and the same wavelengths. We can now compare the conversion efficiencies of both types of OPO with the same CW threshold using the SROPO implicit equation (16) of [14] with $R = R_{\text{SROPO}}$. As seen in Fig. 2, the efficiency of the SROPO grows faster just above threshold until it reaches complete pump depletion for $I_p \simeq 1.9\, I_{\text{th}}^{\text{CW}}$. This optimal normalized pump intensity, which can be evaluated with (24a) in [14], is different from the value of $\pi^2/4 \simeq 2.4$ usually considered in SROPO because of the low cavity finesse with $R_{\text{SROPO}} \simeq 0.16$. Then, for input pump intensity higher than this value, part of the signal and idler is converted back into pump in the nonlinear crystal and the SROPO efficiency decreases. Such a back-conversion effect is a well-known limit to the conversion efficiency of pulsed SROPOs [16, 17, 20]. On the other hand, such a detrimental effect is not observed with the BWOPO where the CW conversion efficiency presents a monotonic growth with an asymptotic limit of 1 for high pumping rates, without the occurrence of back-conversion.

2.3. Pulsed regime

In addition to the steady-state conversion efficiency, another important effect for the overall efficiency in pulsed regime is the build-up of the oscillation from quantum noise during which

the pump intensity is not significantly depleted. To derive an analytic expression of the build-up time, we have to further simplify the coupled-wave equations (5a)–(5c) which involve space and time partial derivatives. First, we neglect pump depletion during build-up which enables to reduce the system to (5a) and (5b) with the pump amplitude as a driving term. Secondly, we assume that the characteristic timescale of the pulses is longer than the propagation delay through the nonlinear crystal, $\tau = L/v_g$, so that space and time profiles can be factorized as separated functions with the longitudinal profiles determined with CW-regime solutions. With these two assumptions, the amplitudes of the three waves read:

$$A_b(z,t) = a_b(t)\cos\left[\pi z/(2L)\right], \tag{32a}$$

$$A_f(z,t) = a_f(t)\sin\left[\pi z/(2L)\right], \tag{32b}$$

$$A_p(z,t) = \pi/(2\kappa L)\sqrt{I_p(t)\,/I_{\mathrm{th}}^{\mathrm{CW}}}, \tag{32c}$$

where the longitudinal profiles correspond to CW solutions at threshold. Inserting amplitude profiles (32a)–(32c) in coupled equations (5a) and (5b) and carrying out integration over z, the following set of two coupled equations involving only time derivatives is obtained:

$$a_b(t) + \frac{2\tau}{\pi}\frac{\mathrm{d}a_b(t)}{\mathrm{d}t} = \sqrt{I_p/I_{\mathrm{th}}^{\mathrm{CW}}}\,a_f^*(t)\,, \tag{33a}$$

$$a_f(t) + \frac{2\tau}{\pi}\frac{\mathrm{d}a_f(t)}{\mathrm{d}t} = \sqrt{I_p/I_{\mathrm{th}}^{\mathrm{CW}}}\,a_b^*(t)\,. \tag{33b}$$

For a step-wise pump temporal profile with the pump intensity switched on to a constant value, I_p, at $t = 0$, the solution in terms of intensity, $I_{b,f} \propto \left|a_{b,f}\right|^2$, is

$$I_{b,f}(t) = I_{b,f}(0)\exp\left(t/\tau_{\mathrm{BWOPO}}\right), \tag{34}$$

with

$$\frac{1}{\tau_{\mathrm{BWOPO}}} = \frac{\pi}{\tau}\left(\sqrt{\frac{I_p}{I_{\mathrm{th}}^{\mathrm{CW}}}} - 1\right). \tag{35}$$

The oscillation build-up time is defined as the time to reach a detectable intensity level, I_{det}, starting from the quantum noise characterized by the equivalent intensity level, I_{noise}:

$$\tau_{\mathrm{bu}} = \frac{\tau\, g_{\mathrm{Log}}}{\pi\left(\sqrt{I_p/I_{\mathrm{th}}^{\mathrm{CW}}} - 1\right)}, \tag{36}$$

with

$$g_{\mathrm{Log}} = \ln\left(\frac{I_{\mathrm{det}}}{I_{\mathrm{noise}}}\right). \tag{37}$$

The duration of the build-up time is thus proportional to g_{Log} whose value depends on the detection sensitivity, the mode volume, and other experimental parameters. Conversely to the CW regime, the threshold definition in pulsed regime is thus somewhat arbitrary. For the calculations presented in the following, we set $g_{\mathrm{Log}} = 18$, as in [16]. However, the value of g_{Log} is straightforwardly adjustable to be more relevant for other conditions. Moreover, one could note that a variation of the noise or detection level over more than an order of magnitude only induces a 10 % variation of the g_{Log} value.

The comparison with the SROPO can be continued for the build-up time. In the case of a SROPO with the same CW threshold as the BWOPO, i.e. $R = R_{\mathrm{SROPO}}$ with R_{SROPO} defined in (31), and with cavity mirrors directly located on the crystal facets so that the cavity round-trip

time τ_{cav} is equal to 2τ, the SROPO build-up time can be determined from (A6) (see Appendix) as follows:

$$\tau_{\mathrm{bu,SROPO}} = \tau g_{\mathrm{Log}} \left\{ \ln\left[\cosh\left(\frac{\pi}{2}\sqrt{\frac{I_p}{I_{\mathrm{th}}^{\mathrm{CW}}}}\right)\right] - \ln\left[\cosh\left(\frac{\pi}{2}\right)\right] \right\}^{-1}. \tag{38}$$

The latter expression can be approximated with an accuracy better than 10% using the approximation $\cosh(x) \simeq \exp(x)/2$, which yields:

$$\tau_{\mathrm{bu,SROPO}} \simeq \frac{2\tau\, g_{\mathrm{Log}}}{\pi\left(\sqrt{I_p/I_{\mathrm{th}}^{\mathrm{CW}}} - 1\right)} = 2\tau_{\mathrm{bu}}. \tag{39}$$

Whatever the input pump intensity, the build-up time of the BWOPO is thus typically two times shorter than the one of the considered "equivalent" SROPO. This is indeed confirmed in Fig. 3 where we also indicate estimated values for OPO setups based on typical parameters ($I_{\mathrm{th}}^{\mathrm{CW}} = 75\,\mathrm{MW/cm^2}$ and $\tau = 44.3\,\mathrm{ps}$). In Fig. 3, the build-up times calculated respectively with formulas (36) and (38) are also compared with FDTD numerical simulations, where the coupled nonlinear equations (5a)–(5c) are solved as explained in Section 3.3, except that we inject here a constant intensity instead of a random noise for an easier evaluation of the oscillation threshold criterion and consider here a step-wise pump temporal profile. The value of the build-up time provided by the analytic evaluation of the BWOPO is higher than the one obtained by numerical calculation. Nonetheless, except for peak intensities close to the CW threshold where there is a factor of two between numerical and analytical evaluations, the difference between the two values reduces rapidly to be less than 25 % for $I_p > 2I_{\mathrm{th}}^{\mathrm{CW}}$ despite the relatively strong assumptions made to derive the analytic expression.

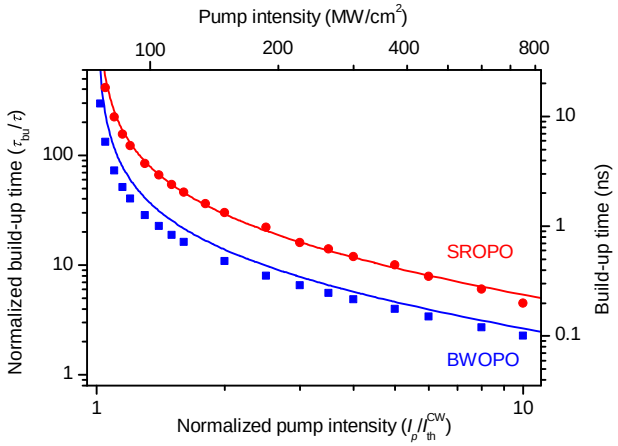

Fig. 3. Build-up time of BWOPO and SROPO (with $R_{\mathrm{SROPO}} = 1/\cosh^2(\pi/2)$ and $\tau_{\mathrm{cav}} = 2\tau$) as functions of the pump intensity normalized to the CW threshold intensity (solid lines: analytic formulas with $g_{\mathrm{Log}} = 18$; symbols: numerical simulation). The left axis provides the build-up time, τ_{bu}, normalized to the light propagation time, τ, through the nonlinear medium while the right axis gives the corresponding values for a typical nonlinear crystal with $L = 7\,\mathrm{mm}$ and $n_g = 1.9$ (i.e., $\tau = 44.3\,\mathrm{ps}$). The pump intensity of the top axis is evaluated for a typical CW threshold intensity $I_{\mathrm{th}}^{\mathrm{CW}} = 75\,\mathrm{MW/cm^2}$.

2.3.1. Square temporal profile

For a square temporal profile of duration $\overline{\tau}_p$, one can derive from (36) the pulsed peak intensity to reach a detectable level of generated radiation at the trailing edge of the pump pulse:

$$\overline{I}_{\mathrm{th}}^{\mathrm{peak}} = I_{\mathrm{th}}^{\mathrm{CW}} \left(1 + \frac{\tau}{\pi \overline{\tau}_p} g_{\mathrm{Log}}\right)^2. \tag{40}$$

The corresponding threshold fluence is thus

$$\overline{J}_{\mathrm{th}} = \overline{\tau}_p \left(1 + \frac{\tau}{\pi \overline{\tau}_p} g_{\mathrm{Log}}\right)^2 I_{\mathrm{th}}^{\mathrm{CW}}. \tag{41}$$

The latter expression provides a first estimation of the threshold fluence for a given pulse duration. Expression (41) has a minimum for pulse duration $\overline{\tau}_{p,\mathrm{opt}}$ which satisfies $\mathrm{d}\overline{J}_{\mathrm{th}}/\mathrm{d}\overline{\tau}_p = 0$:

$$\overline{\tau}_{p,\mathrm{opt}} = \tau \, g_{\mathrm{Log}}/\pi, \tag{42}$$

with the corresponding minimum of the threshold fluence:

$$\overline{J}_{\mathrm{th,min}} = 4 I_{\mathrm{th}}^{\mathrm{CW}} \, \tau \, g_{\mathrm{Log}}/\pi, \tag{43}$$

which corresponds to a peak power of 4 times the CW threshold power over a duration of 4.7τ.

The pulsed threshold peak intensity can be derived in the same way for the equivalent SROPO from (38) or its approximation (39). The ratio between pulsed threshold peak intensities of the BWOPO and its equivalent SROPO can then be written as

$$\frac{\overline{I}_{\mathrm{th,SROPO}}^{\mathrm{peak}}}{\overline{I}_{\mathrm{th}}^{\mathrm{peak}}} \simeq \frac{\pi \overline{\tau}_p + 2\tau g_{\mathrm{Log}}}{\pi \overline{\tau}_p + \tau g_{\mathrm{Log}}}. \tag{44}$$

The ratio of the pulsed threshold peak intensities is thus between 1 for long pulse durations, where the conditions become close to the CW regime, and 2 for short pulses. However, this must be balanced by the fact that the considered equivalent SROPO is not representative of a typical SROPO based on a higher finesse cavity whose threshold intensity would actually be lower.

As in [16], we can derive an approximate expression of the pulsed conversion efficiency. For this purpose, we assume that the temporal profile of the output divides into two distinct temporal phases in the same manner as in [20]. The first one is the BWOPO buildup phase, during which the pump is assumed constant and whose duration is τ_{bu}. The second one is the steady-state regime where all the intensities are known and are identical to continuous-wave regime solutions derived in Sec. 2.2. We can hence write

$$\overline{\eta}_{\mathrm{pulse}} = \frac{\overline{\tau}_p - \tau_{\mathrm{bu}}}{\overline{\tau}_p} \eta, \tag{45}$$

where η is given by (23) and τ_{bu} by (36). The value of $\overline{\eta}_{\mathrm{pulse}}$ can then be numerically evaluated by solving (45). If one also approximate η by its asymptotic value for strong pumping (29), an analytical formula can be derived for a square temporal pulse profile:

$$\overline{\eta}_{\mathrm{pulse}} = \left[1 - \frac{\tau \, g_{\mathrm{Log}}}{\overline{\tau}_p \pi \left(\sqrt{\overline{I}_p^{\mathrm{peak}}/I_{\mathrm{th}}^{\mathrm{CW}}} - 1\right)}\right] \left[1 - 16 \exp\left(-\pi \sqrt{\overline{I}_p^{\mathrm{peak}}/I_{\mathrm{th}}^{\mathrm{CW}}}\right)\right]. \tag{46}$$

The above equation can also be expressed in terms of pump fluence $\overline{J} = \overline{\tau}_p \overline{I}_p^{\mathrm{peak}}$.

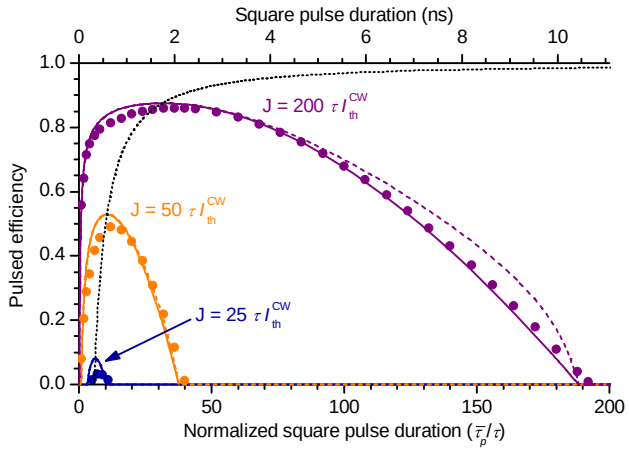

Fig. 4. BWOPO conversion efficiency as a function of the pulse duration for a square pulse profile and several pump fluences (solid lines: calculation with (45) with $g_{\mathrm{Log}} = 18$; dashed lines: approximated expression (46); symbol: numerical simulation). The bottom axis provides the square pulse duration, $\overline{\tau}_p$, normalized to the light propagation time, τ, through the nonlinear medium while the top axis gives the corresponding values for a typical nonlinear crystal with $L = 7$ mm and $n_g = 1.9$ (i.e., $\tau \simeq 44.3$ ps). For a typical CW threshold intensity $I_{\mathrm{th}}^{\mathrm{CW}} = 75\,\mathrm{MW/cm^2}$, the three considered pump fluences are respectively 0.083, 0.166, and 0.665 J/cm^2. The black dotted line provides the optimum duration and corresponding pulsed efficiency for increasing fluences.

Fig. 4 shows the pulsed conversion efficiency evaluated with expression (45) and its approximation (46) as a function of the pulse duration for constant pump fluences. The agreement between the two expressions is excellent for pulse duration leading to peak intensities which are high enough for (29) to be accurate; i.e., better than 10 % for $\overline{\tau}_p < 0.62\,\overline{J}/I_{\mathrm{th}}^{\mathrm{CW}}$. The estimation remains nevertheless reasonable for longer pulse lengths.

Analytic evaluation of the pulsed efficiency is also compared with results obtained from numerical simulations in Fig. 4. The largest discrepancy is observed at short pulse durations where the assumption of a characteristic timescale longer than τ, used to derive the analytic formulas, is not valid. The agreement remains nevertheless quite good despite the pulse profiles shown in Fig. 5(a) where steady-state is far from being reached during the pulse duration. On the other hand, as expected, an excellent agreement is obtained in Fig. 4 for pulses lengths corresponding to Fig. 5(b) and (c) where transient modulations only occurs during a relatively short duration.

For a given pump fluence, the optimum of efficiency results from a balance between the minimization of the energy lost during the build up phase during which the optimal peak power is 4 times the CW threshold and the maximization of the steady-state conversion efficiency which requires the highest possible peak power. For the pump fluences considered in Fig. 4, the corresponding optimal pump peak power is respectively 4.07, 4.71 and $6.37 \times I_{\mathrm{th}}^{\mathrm{CW}}$.

Fig. 6 presents the BWOPO efficiency as a function of the pump peak intensity for various pulse durations. This illustrates the effect of the build-up time on the oscillation threshold and efficiency. It can also be noticed that the BWOPO operation is expected to be close to the CW limit for pulse durations longer than typically $100\,\tau$, which corresponds to a few nanoseconds for typical crystal parameters.

The impact of the quantum noise fluctuations on the pulsed conversion efficiency stability can

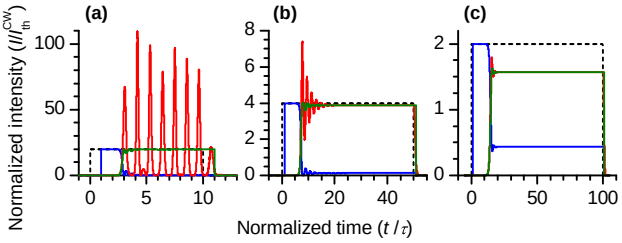

Fig. 5. Temporal profiles of input pump (dashed black line), depleted pump (blue line), forward (green line), and backward (red line) pulses corresponding to calculated efficiency in Fig. 4 for $J = 200\,\tau I_{\rm th}^{\rm CW}$ for incident pump pulse durations of (a) $\overline{\tau}_p = 10\,\tau$, (b) $50\,\tau$, and (c) $100\,\tau$.

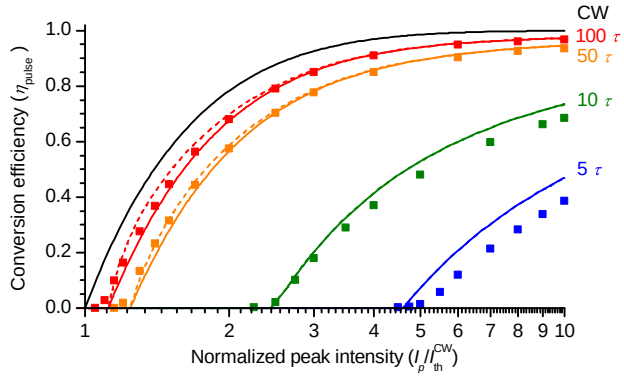

Fig. 6. BWOPO conversion efficiency as a function of the pump peak intensity for a square pulse profile and several durations (solid lines: calculation with (45) with $g_{\rm Log} = 18$; dashed lines: approximated expression (46); symbol: numerical simulation). For a typical nonlinear crystal with $L = 7$ mm and $n_g = 1.9$ (i.e., $\tau \simeq 44.3$ ps), the considered durations are respectively 0.22, 0.44, 2.21 and 4.43 ns.

be evaluated by differentiation of (45) with respect to $I_{\rm noise}$. After some algebra, one can write

$$\frac{{\rm d}\overline{\eta}_{\rm pulse}}{\overline{\eta}_{\rm pulse}} = \frac{{\rm d}I_{\rm noise}}{I_{\rm noise}} \frac{1}{\left(\pi\overline{\tau}_p/\tau + g_{\rm Log}\right)\left(\sqrt{\overline{I}_p^{\rm peak}/\overline{I}_{\rm th}^{\rm peak}} - 1\right)}, \tag{47}$$

where (37) and (40) were used for the derivation of the latter expression. As expected, a higher output fluence instability is awaited close to the oscillation threshold. In addition, the shorter is the pulse duration, the higher is the anticipated fluctuation magnitude. This feature is related to the higher relative impact of the buildup time fluctuation on the pulsed efficiency for shorter pulses. For a given pumping ratio and with $\tau = 44.3$ ps, it is thus expected to reduce the fluctuation by typically an order of magnitude by increasing the pulse duration from 200 ps to 5 ns. This trend is confirmed by numerical simulation carried out with a random initial noise for various pulse durations (not shown here). A similar analysis could straightforwardly be carried out to evaluate the influence of pump intensity or pulse duration fluctuations.

2.3.2. Gaussian pulse profile

To derive the pulsed threshold formula, we chose the same convention as Brosnan and Byer [12] to define the Gaussian pulse profile:

$$I_p(t) = I_p^{\text{peak}} \exp\left(-2t^2/\tau_p^2\right). \tag{48}$$

Also similarly to Brosnan and Byer, we introduce an equivalent square pulse profile whose duration $\overline{\tau}_p$ corresponds to the time during which the instantaneous power is higher than the CW threshold power, i.e. $I_p(t) > I_{\text{th}}^{\text{CW}}$. One obtains:

$$\overline{\tau}_p = \tau_p \sqrt{2 \ln\left(I_p^{\text{peak}}/I_{\text{th}}^{\text{CW}}\right)}. \tag{49}$$

For the peak power $\overline{I}_p^{\text{peak}}$ of the equivalent square pulse, it is defined such as the overall gain experienced by the forward and backward waves is similar to one provided by the Gaussian pulse when $I_p(t) > I_{\text{th}}^{\text{CW}}$. From (33), this yields to the following relation

$$\overline{\tau}_p \sqrt{\overline{I}_p^{\text{peak}}} = \sqrt{I_p^{\text{peak}}} \int_{-\overline{\tau}_p/2}^{\overline{\tau}_p/2} \exp\left(-t^2/\tau_p^2\right) \mathrm{d}t, \tag{50}$$

where $\overline{\tau}_p$ is given by (49). One thus obtains

$$\overline{I}_p^{\text{peak}} = I_p^{\text{peak}} \frac{\pi}{4} \left\{ \frac{\operatorname{erf}\left[\overline{\tau}_p/(2\tau_p)\right]}{\overline{\tau}_p/(2\tau_p)} \right\}^2, \tag{51}$$

with

$$\operatorname{erf}(\tau) = \frac{2}{\sqrt{\pi}} \int_0^{\tau} \exp\left(-t^2\right) \mathrm{d}t. \tag{52}$$

The equivalent-square-pulse intensity at the pulsed oscillation threshold $\overline{I}_{\text{th}}^{\text{peak}}$ has to satisfy (40) and the corresponding threshold peak intensity of the Gaussian pulse $I_{\text{th}}^{\text{peak}}$ is related to $\overline{I}_{\text{th}}^{\text{peak}}$ through (51). For a given pulse duration τ_p, it is thus possible to numerically evaluate the threshold peak intensity of the Gaussian pulse by solving the closed system provided by (40), (49), and (51). The corresponding threshold fluence of the Gaussian pulse is then given by

$$J_{\text{th}} = \sqrt{\frac{\pi}{2}} I_{\text{th}}^{\text{peak}} \tau_p. \tag{53}$$

The threshold fluence from (53) is plotted in Fig. 7 as a function of the Gaussian pulse duration. The minimal fluence is obtained for a duration of typically 3τ, a fluence of $25\tau I_{\text{th}}^{\text{CW}}$, and a corresponding peak power $I_{\text{th}}^{\text{peak}} = 6.6\, I_{\text{th}}^{\text{CW}}$.

However, the latter evaluation of the threshold fluence requires to numerically solve several equations and a more straightforward way to estimate the threshold peak intensity and fluence for the Gaussian pulse would be more convenient for practical use. For this purpose, as in Brosnan–Byer's analysis, we assume that $\overline{\tau}_p = 2\tau_p$, which enables to derive a simple expression of the threshold peak intensity:

$$I_{\text{th}}^{\text{peak}}\left(\overline{\tau}_p = 2\tau_p\right) = \frac{4}{\pi \operatorname{erf}^2(1)} \left(1 + \frac{\tau}{2\pi\tau_p} g_{\text{Log}}\right)^2 I_{\text{th}}^{\text{CW}}. \tag{54}$$

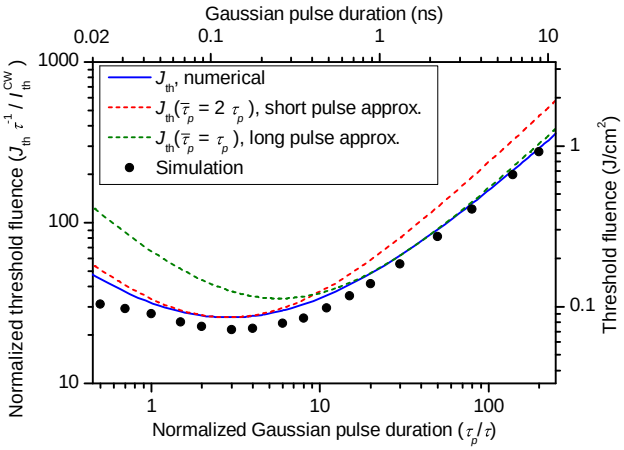

Fig. 7. Threshold fluence of BWOPO as a function of pulse duration for a Gaussian pulse profile. The pump intensity is normalized to the CW threshold intensity (solid blue line: numerical solution of (40), (49), and (50) with $g_{\mathrm{Log}} = 18$; dashed red line: analytic formula (55) for short pulses; dashed green line: analytic formula (57) for long pulses; symbols: numerical simulation). The left axis provides the build-up time, τ_{bu}, normalized to the light propagation time, τ, through the nonlinear medium while the right axis gives the corresponding values for a typical nonlinear crystal with $L = 7$ mm and $n_g = 1.9$ (i.e., $\tau \simeq 44.3$ ps).

We can then use (53) to determine the corresponding threshold fluence

$$J_{\mathrm{th}}\left(\overline{\tau}_p = 2\tau_p\right) = 2.25\,\tau_p \left(1 + \frac{g_{\mathrm{Log}}\, n_g\, L}{2\pi\, \tau_p\, c}\right)^2 I_{\mathrm{th}}^{\mathrm{CW}}, \tag{55}$$

with $\tau = n_g L/c$ and where we use the numerical evaluation of the factor $2\sqrt{2}/\left[\sqrt{\pi}\,\mathrm{erf}^2\,(1)\right] = 2.25$. One could notice that the Gaussian pulse threshold fluence provided by (55) is actually close to threshold fluence for a square pulse profile (41): $J_{\mathrm{th}}\left(\overline{\tau}_p = 2\tau_p\right) = 1.125\,\overline{J}_{\mathrm{th}}$. Moreover, as seen in Fig. 7, the accuracy of (54) and (55) is the highest close to the pulse duration leading to the minimal threshold fluence; i.e., $\tau_{p,\mathrm{opt}} = \tau\, g_{\mathrm{Log}}/(2\pi)$

For longer pump pulses, a better accuracy is obtained assuming $\overline{\tau}_p = \tau_p$. The corresponding approximated expressions are then:

$$I_{\mathrm{th}}^{\mathrm{peak}}\left(\overline{\tau}_p = \tau_p\right) = \frac{1}{\pi\,\mathrm{erf}^2\,(1/2)} \left(1 + \frac{\tau}{\pi\tau_p} g_{\mathrm{Log}}\right)^2 I_{\mathrm{th}}^{\mathrm{CW}}, \tag{56}$$

and

$$J_{\mathrm{th}}\left(\overline{\tau}_p = \tau_p\right) = 1.47\,\tau_p \left(1 + \frac{g_{\mathrm{Log}}\, n_g\, L}{\pi\, \tau_p\, c}\right)^2 I_{\mathrm{th}}^{\mathrm{CW}}, \tag{57}$$

where we use the numerical evaluation of the factor $1/\left[\sqrt{2\pi}\,\mathrm{erf}^2\,(1/2)\right] = 1.47$.

Threshold fluences determined by numerical simulation are also shown in Fig. 7. A very good agreement with approximate expression (57) is obtained for pulse durations longer than typically 30τ. For pulse shorter than 10τ it is more accurate to use approximate expression (55) with a relative difference of typically 20 % down to duration shorter than τ where the assumptions made to derive expressions (53) and (55) are too invalid. For such short pulse durations the threshold fluence determined by numerical simulation grows more slowly than the one provided by the

expressions when the duration shortens. The discrepancy remains nonetheless still reasonable (less than a factor 2).

To further assess the relevance of our model, we compare experimental values of the peak intensity at threshold, reported in the literature for two different pulse durations (47 ps and 13 ns), with $I_{\mathrm{th}}^{\mathrm{peak}}$, determined by solving the closed system provided by (40), (49), and (51), and its approximations $I_{\mathrm{th}}^{\mathrm{peak}}\left(\overline{\tau}_p = 2\tau_p\right)$ and $I_{\mathrm{th}}^{\mathrm{peak}}\left(\overline{\tau}_p = \tau_p\right)$, respectively given by expressions (54) and (56). As shown in Table 1, a good agreement (better than 5 %) between experimental values and $I_{\mathrm{th}}^{\mathrm{peak}}$ is obtained for both pulse durations assuming $d_{\mathrm{eff}} = 8$ pm/V and with $g_{\mathrm{Log}} = 18$. As expected, $I_{\mathrm{th}}^{\mathrm{peak}}\left(\overline{\tau}_p = 2\tau_p\right)$ is more accurate than $I_{\mathrm{th}}^{\mathrm{peak}}\left(\overline{\tau}_p = \tau_p\right)$ for the shortest pulse duration and conversely for the longest pulse duration. The threshold expressions provided by our model might thus be useful for the practical design of BWOPOs.

Table 1. **Measured threshold peak intensities of pulsed BWOPO reported in the literature and corresponding theoretical values determined with the expressions derived in this work.** $d_{\mathrm{eff}} = 8$ **pm/V is assumed for the calculation of** $I_{\mathrm{th}}^{\mathrm{CW}}$**.**

Experiment		
L_c	5 mm	7 mm
τ_p	47 ps	13 ns
$I_{\mathrm{th,experiment}}^{\mathrm{peak}}$	1.6 GW/cm^2	83 MW/cm^2
Reference	[2]	[11]
Theory		
$I_{\mathrm{th}}^{\mathrm{CW}}$	101 MW/cm^2	71.5 MW/cm^2
$I_{\mathrm{th}}^{\mathrm{peak}}$	1.52 GW/cm^2	80.4 MW/cm^2
$I_{\mathrm{th}}^{\mathrm{peak}}\left(\overline{\tau}_p = 2\tau_p\right)$	1.56 GW/cm^2	130.6 MW/cm^2
$I_{\mathrm{th}}^{\mathrm{peak}}\left(\overline{\tau}_p = \tau_p\right)$	2.81 GW/cm^2	87.3 MW/cm^2

3. Linewidth

3.1. Phase-matching acceptance bandwidth

As shown by Canalias and Pasiskevicius [2], the BWOPO exhibits peculiar spectral properties with the generation of a very narrow backward radiation while the spectral content of the pump is transferred to the forward wave. For a narrow, Fourier-transform limited pump it is thus expected that both the backward and the forward waves have a narrow spectral linewidth.

Assuming that quasi-phase matching is satisfied for angular frequencies ω_p, ω_b, and ω_f with $\omega_p = \omega_b + \omega_f$, the magnitude of the phase mismatch, $\Delta k(\Delta\omega)$, for frequencies $\omega_b' = \omega_b + \Delta\omega$ and $\omega_f' = \omega_f - \Delta\omega$ is given by

$$\Delta k(\Delta\omega) = k(\omega_b + \Delta\omega) - k(\omega_b) - k\left(\omega_f - \Delta\omega\right) + k\left(\omega_f\right) \tag{58}$$

A first order Taylor expansion yields

$$\Delta k(\Delta\omega) = \left(\frac{1}{v_{gb}} + \frac{1}{v_{gf}}\right)\Delta\omega, \tag{59}$$

The difference-frequency generation (DFG) bandwidth for backward interaction, defined by the condition $\Delta k L/2 = \pi$, thus reads in terms of frequency, $\nu = \omega/(2\pi)$, rather than angular frequency

$$\Delta\nu_{\mathrm{BWDFG}} = \frac{c}{2n_g L}, \tag{60}$$

where n_g is the average group index, $n_g = \left(n_{gb} + n_{gf}\right)/2$.

One can compare the latter expression with the same definition of the DFG acceptance bandwidth for forward interaction:

$$\Delta\nu_{\mathrm{FWDFG}} = \frac{c}{\Delta n_g L}, \tag{61}$$

where Δn_g is the group index difference between signal and idler, $\Delta n_g = \left|n_{gs} - n_{gi}\right|$.

For similar crystal lengths, the ratio of the two bandwidth is thus given by

$$\frac{\Delta\nu_{\mathrm{FWDFG}}}{\Delta\nu_{\mathrm{BWDFG}}} = \frac{2n_g}{\Delta n_g}. \tag{62}$$

In terms of DFG acceptance bandwidth, backward interaction is thus equivalent to forward interaction in a nonlinear medium with a "giant" group index difference equal to $2n_g$. If one consider typical values $n_g = 1.9$ and $\Delta n_g = 0.02$ [4], the acceptance bandwidth for backward interaction is thus more than a hundred times narrower than for forward interaction, as pointed out in early backward DFG experiments [21]. This narrow acceptance bandwidth is very promising to generate Fourier-transform-limited pulses (at both ω_b and ω_f) from a backward OPO without any additional spectral filtering, provided that the pump spectrum is also narrow.

3.2. Optical parametric amplifier bandwidth

To derive the OPA gain spectrum, we solve the coupled-wave equations in CW regime under the undepleted pump approximation where we now consider imperfect phase-matching:

$$\frac{\mathrm{d}A_b}{\mathrm{d}z} = -i\kappa A_{p0} A_f^* \exp\left(i\Delta k z\right), \tag{63a}$$

$$\frac{\mathrm{d}A_f}{\mathrm{d}z} = i\kappa A_{p0} A_b^* \exp\left(i\Delta k z\right), \tag{63b}$$

where $A_p\left(z\right) = A_p\left(0\right) = A_{p0}$ and $\Delta k = k_p - k_f + k_b - K_G$. We assume that there is no input for the backward wave, i.e. $A_b\left(L\right) = 0$, and that there is an input for the forward wave. After solving the system (63) under these assumptions, one obtains the expression of the output forward amplitude

$$\begin{aligned} A_f\left(L\right) = {} & A_f\left(0\right)\left(4\kappa^2\left|A_{p0}\right|^2 + \Delta k^2\right)^{1/2} e^{i\,\Delta k\,L/2} \Bigg/ \left\{\left(4\kappa^2\left|A_{p0}\right|^2 + \Delta k^2\right)^{1/2}\right. \\ & \left.\times\cos\left[\left(4\kappa^2\left|A_{p0}\right|^2 + \Delta k^2\right)^{1/2} L/2\right] + i\,\Delta k\,\sin\left[\left(4\kappa^2\left|A_{p0}\right|^2 + \Delta k^2\right)^{1/2} L/2\right]\right\} \end{aligned} \tag{64}$$

The gain for the forward intensity, $\left|A_f\left(L\right)\right|^2 / \left|A_f\left(0\right)\right|^2 = 1 + G_{\mathrm{BWOPA}}$, can be determined to be

$$G_{\mathrm{BWOPA}} = \frac{\sin^2\left[\left(\pi/2\right)\left(I_p/I_{\mathrm{th}}^{\mathrm{CW}} + \Delta k^2 L^2/\pi^2\right)^{1/2}\right] I_p/I_{\mathrm{th}}^{\mathrm{CW}}}{\cos^2\left[\left(\pi/2\right)\left(I_p/I_{\mathrm{th}}^{\mathrm{CW}} + \Delta k^2 L^2/\pi^2\right)^{1/2}\right] I_p/I_{\mathrm{th}}^{\mathrm{CW}} + \Delta k^2 L^2/\pi^2}, \tag{65}$$

where the incident pump intensity I_p is normalized by the BWOPO threshold (19). For $\Delta k = 0$, one can notice that G_{BWOPA} tends to infinity when $I_p \to I_{\mathrm{th}}^{\mathrm{CW}}$, which is consistent with the onset of the parametric oscillation. On the other hand, as soon as $\Delta k \neq 0$, there is no value of the pump intensity that makes the denominator in (65) equal to zero and it is thus not possible to reach oscillation since

$$G_{\mathrm{BWOPA}} \leq \frac{\pi^2}{\Delta k^2 L^2} \frac{I_p}{I_{\mathrm{th}}^{\mathrm{CW}}}. \tag{66}$$

This feature is a *very* particular characteristic of the BWOPO that differs from the conventional forward OPO where the small-signal gain can be larger than the cavity loss for phase-mismatched interactions if the pump intensity is high enough.

When I_p approaches $I_{\mathrm{th}}^{\mathrm{CW}}$ and for a small phase mismatch, (65) can be approximated by the following expression:

$$G_{\mathrm{BWOPA}} \simeq \frac{4}{\pi^2 \left(1 - \sqrt{I_p / I_{\mathrm{th}}^{\mathrm{CW}}}\right)^2 + 4\Delta k^2 L^2 / \pi^2}. \tag{67}$$

It is then straightforward to derive the phase-mismatch acceptance, $\Delta k_{\mathrm{BWOPA}}$, at half maximum of the BWOPA gain given by (67), which reads

$$\Delta k_{\mathrm{BWOPA}} = \frac{\pi^2}{2L} \left(1 - \sqrt{I_p / I_{\mathrm{th}}^{\mathrm{CW}}}\right). \tag{68}$$

The accuracy of above approximation is better than 10% for $I_p > 0.35 I_{\mathrm{th}}^{\mathrm{CW}}$, compared to the bandwidth derived by numerical calculation with (65).

As for threshold and efficiency, we can compare the backward OPA bandwidth with its forward interaction analog. For this purpose, we consider the sub-threshold SROPO or cavity-enhanced forward OPA (CE-FWOPA) with an equivalent mirror reflectivity R_{SROPO} given by (31) leading to the same CW oscillation threshold as the BWOPO. The corresponding CE-FWOPA gain reads (see Appendix):

$$\begin{aligned} G_{\mathrm{CE-FWOPA}} = {} & \sinh^2\left(\frac{\pi}{2}\right) \\ & \times \sinh^2\left[\frac{\pi}{2}\left(\frac{I_p}{I_{\mathrm{th}}^{\mathrm{CW}}} - \frac{\Delta k^2 L^2}{\pi^2}\right)^{1/2}\right] \frac{I_p}{I_{\mathrm{th}}^{\mathrm{CW}}} \Bigg/ \Bigg(\cosh^2\left(\frac{\pi}{2}\right)\left(\frac{I_p}{I_{\mathrm{th}}^{\mathrm{CW}}} - \frac{\Delta k^2 L^2}{\pi^2}\right)^{1/2} \\ & - \left\{\cosh^2\left[\frac{\pi}{2}\left(\frac{I_p}{I_{\mathrm{th}}^{\mathrm{CW}}} - \frac{\Delta k^2 L^2}{\pi^2}\right)^{1/2}\right] \frac{I_p}{I_{\mathrm{th}}^{\mathrm{CW}}} - \frac{\Delta k^2 L^2}{\pi^2}\right\}^2\Bigg)^2. \end{aligned} \tag{69}$$

In same way as for the BWOPA gain, one can derive an approximate expansion of (69) for I_p close to $I_{\mathrm{th}}^{\mathrm{CW}}$ and for small phase mismatch:

$$G_{\mathrm{CE-FWOPA}} \simeq \frac{4 \sinh^2(\pi/2)}{\left\{\pi\left(1 - \sqrt{I_p / I_{\mathrm{th}}^{\mathrm{CW}}}\right) + \left[\pi/2 - \tanh(\pi/2)\right] \Delta k^2 L^2 / \pi^2\right\}^2}. \tag{70}$$

The corresponding phase-mismatch acceptance at half maximum of $G_{\mathrm{CE-FWOPA}}$ is given by

$$\Delta k_{\mathrm{CE-FWOPA}} = \frac{\pi}{L}\left[\frac{2\left(\sqrt{2} - 1\right)}{1 - (2/\pi)\tanh(\pi/2)}\right]^{1/2} \left(1 - \sqrt{I_p / I_{\mathrm{th}}^{\mathrm{CW}}}\right)^{1/2}. \tag{71}$$

To have an accuracy better than 10% compared to numerical calculation with (69) the pump intensity must satisfy: $I_p > 0.7 I_{\text{th}}^{\text{CW}}$.

Including the group index scaling factor provided by (62), the ratio of the two OPA bandwidths (71) and (68), expressed in terms of frequency bandwidth is given by

$$\frac{\Delta\nu_{\text{CE-FWOPA}}}{\Delta\nu_{\text{BWOPA}}} = 0.9 \times \frac{2n_g/\Delta n_g}{\left(1-\sqrt{I_p/I_{\text{th}}^{\text{CW}}}\right)^{1/2}}, \tag{72}$$

where the leading factor is numerically evaluated for the sake of readability. The analysis of (72) thus reveals that the BWOPA bandwidth narrows faster than the one of the CE-FWOPA when the pump intensity approaches the OPO threshold, i.e. the ratio of the two bandwidths tends to infinity. This means that the very large reduction of the bandwidth that already occurs at low gain is further increased when the pump intensity approaches the oscillation threshold. Fig. 8 illustrates these singular spectral properties for $I_p = 0.95 I_{\text{th}}^{\text{CW}}$ where one can notice that the gain for the CE-FWOPA is basically flat over the full bandwidth of the BWOPA. These features are confirmed in the following for pulsed parametric oscillation.

3.3. Pulsed OPO bandwidth

To extend our investigation of the spectral bandwidth to the case of pulsed OPOs, we carry out FDTD numerical simulations for both the BWOPO and the conventional SROPO under the plane wave approximation; i.e., we numerically solve system (1a)–(1c) for the BWOPO and system (A1a)–(A1c) for the SROPO. The considered simulation parameters are detailed in Table 2. In both case quasi-phase matching is assumed at the carrier frequencies. In the case of the BWOPO, comparable results are obtained with identical group velocities for the three waves, which confirm the relevance of the assumption made for the analytic analysis, i.e. $2n_g \gg \Delta n_g$.

For the conventional forward SROPO, since we consider $\Delta n_g = 0.02$, we have $\Delta\nu_{\text{FWDFG}} = 2.1$ THz for a crystal length $L = 7$ mm. We still consider a SROPO with an equivalent cavity reflectivity given by (31) to have the same CW threshold. We also assume the shortest possible cavity length for the SROPO with mirrors directly on the nonlinear medium ends, i.e. at $z = 0$ and $z = L$.

In both cases, we consider a broadband noise ($\Delta\nu_{\text{noise}} = 40$ THz) characterized by a random

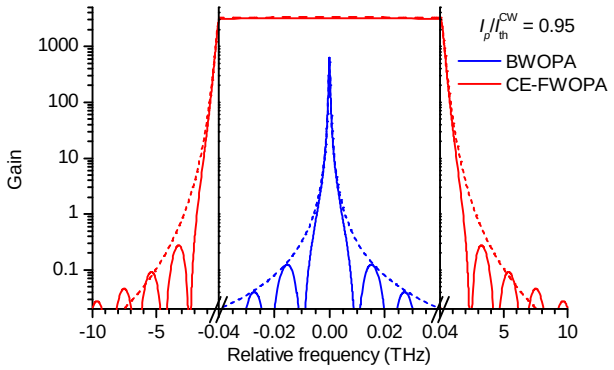

Fig. 8. Gain of the BWOPA and CE-FWOPA as functions of the relative frequency mismatch from perfect phase-matching (solid lines: formulas (65) and (69); dashed lines: approximated expressions (67) and (70)). For the calculation, we set $I_p = 0.95\, I_{\text{th}}^{\text{CW}}$, $n_g = 1.9$, $\Delta n_g = 0.02$, and $L = 7$ mm. Note the change in scale in the middle section of the x-axis.

electric field with a mean value of zero and an equivalent intensity of half a photon per time unit and surface unit.

Table 2. **Parameters used for the numerical simulation of the backward OPO and forward singly resonant OPO.**

Parameter	BWOPO	SROPO
n_{gf}, n_{gs}	1.88	
n_{gb}, n_{gi}	1.90	
n_{gp}	1.92	
L	7 mm	
R	n.a.	0.16
$I_{\text{th}}^{\text{CW}}$	75 MW/cm^2	
Pulse shape	Gaussian	
τ_p (FWHM)	5 ns	
$I_p^{\text{peak}}/I_{\text{th}}^{\text{CW}}$	3	

As shown in Fig. 9, the pulses emitted by the BWOPO exhibit smooth temporal profiles with the emission of a narrow Fourier-transform limited spectum for the forward wave. The spectrum of the backward wave is similarly narrow. To investigate the stability of the output fluence and spectrum, the simulation is carried out 50 times with the same parameters (only the initial random noise changes from pulse to pulse). This leads to relative fluctuation of 0.4 % (standard deviation) of the conversion efficiency of the BWOPO without any observable variations of the forward and backward central wavelength and spectral linewidth. Whatever the spectral distribution of the initial noise, only the forward and backward wavelengths at perfect phase matching oscillate. The only observable variations concern the value of the peak spectral intensity. In the time domain, this is reflected in variations of the pulse build-up time.

On the other hand, as seen in Fig. 10, the SROPO delivers pulses with strong temporal modulations, whose features are consistent with bandwidth and group-velocity effects previously reported in the literature [22]. These modulations display a periodic pattern with a period corresponding to cavity round-trip time. The resulting signal spectrum is thus multimode with a bandwidth of about 800 GHz. As expected, the build-up time of the SROPO is longer that the one of the BWOPO.

The statistics over 50 pulses shows relative fluctuations of a 0.3 % (standard deviation) of the conversion efficiency, which is comparable to the BWOPO. The most striking difference compared to the BWOPO actually concerns the pulse to pulse variations of the spectrum. Indeed, as expected for a SROPO [18], we observe large variations of the power partition between the emitted modes, which are related to the spectral distribution of the initial noise.

This study confirms the very different spectral properties of the BWOPO and the SROPO. While the pump pulse features are the same for the two OPOs and the nonlinear parameters are identical, the BWOPO naturally emits a Fourier-transform-limited spectrum while the SROPO delivers a broadband multimode spectrum. To obtain a Fourier-transform limited emission from the SROPO, one should implement more complex cavity schemes with intracavity spectal filters or based on injection seeding of a narrow-linewidth radiation [23]. On the other hand, the BWOPO deliver a narrow linewidth without any cavity or additional spectral filter.

One should nevertheless keep in mind that our approach considers plane waves in an ideal

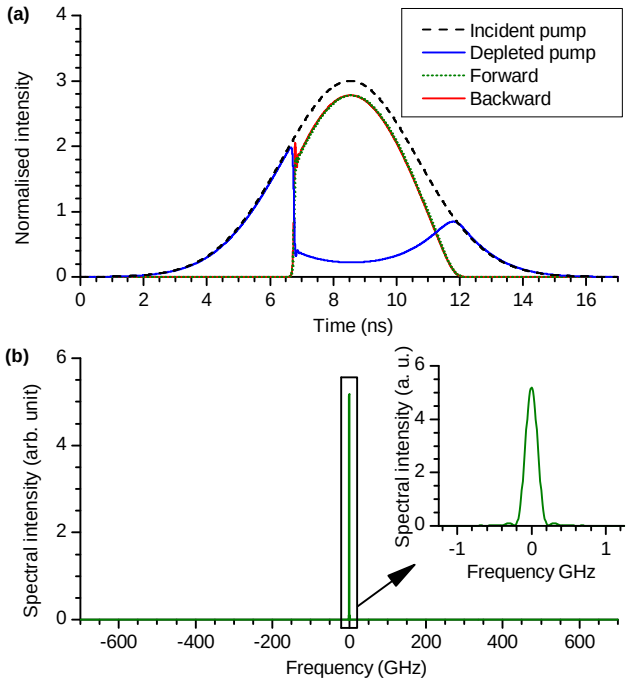

Fig. 9. (a) Temporal profiles of input pump, depleted pump, forward, and backward pulses of the BWOPO calculated by numerical simulation with parameters in Table 2; (b) corresponding spectrum of the forward wave.

QPM nonlinear medium with a monochromatic pump. It would be interesting to extend this work by analyzing the effects of imperfect QPM period while it is expected that a large or non-Fourier-transform-limited pump spectrum would mainly alter the spectrum of the forward wave [4–6]. Another useful outlook would be to develop a more elaborate model to take into account finite beam effects which might alter the BWOPO spectral and spatial profiles. Dedicated experimental studies would also be essential to validate the theoretical results.

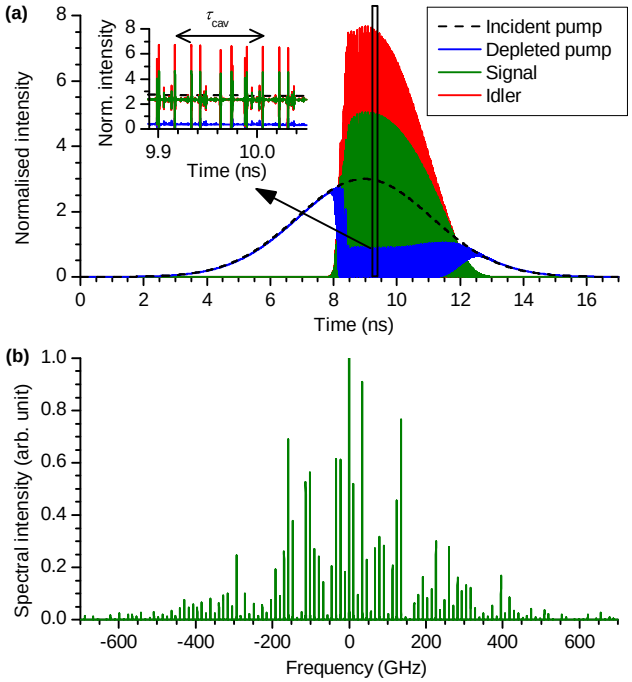

Fig. 10. (a) Temporal profiles of input pump, depleted pump, signal, and idler pulses of the SROPO calculated by numerical simulation with parameters in Table 2; (b) corresponding spectrum of the signal wave.

4. Conclusion

In this paper we have presented the theoretical investigation of the BWOPO in CW and pulsed regime. By exactly taking into account the parametric interaction between the three waves in the nonlinear crystal, our approach has enabled to recover steady-state solutions which are consistent with the literature. Then, we have developed an approach adapted to the description of the pulsed BWOPO oscillation build-up. As the main outcome of this analysis, we have derived an analytic expression of the BWOPO build-up time. Owing to this expression, we have been able to derive a BWOPO analog of the Brosnan–Byer threshold fluence formula for the conventional SROPO. These expressions have then been successfully compared with experimental threshold values reported in the literature. We have also derived an approximate expression of the conversion efficiency in pulsed regime. These expressions can be useful to design a pulsed BWOPO without resorting to extensive numerical simulations. The developed formalism has also been exploited to carry out informative comparisons between the BWOPO and the SROPO. In particular, we show that a SROPO with a coupler reflectivity of about 16 % has the same CW oscillation as the BWOPO based on a similar nonlinear material. This equivalent SROPO has however a build-up time that is typically two times longer than the BWOPO.

We have also study the spectral properties of the BWOPO. A striking result is that the BWOPO oscillation threshold can only be reached at perfect quasi-phase matching and that the subthreshold gain bandwidth is typical several hundreds times narrower than for forward-wave parametric amplification. Numerical simulations of the BWOPO and SROPO pumped by a Fourier-transform-limited nanosecond Gaussian pump pulse have confirmed that the spectral properties of both OPOs are very different. While the SROPO delivers a broadband multimode spectrum, the BWOPO emission is naturally Fourier-transform limited. This unique features is

very promising to implement differential absorption lidar emitters based on BWOPOs for remote gas sensing.

Appendix A: Build-up time and gain bandwidth of the SROPO

A.1. Single-pass FWOPA gain

The coupled nonlinear equations for forward parametric interaction read [23]:

$$\frac{\partial A_i}{\partial z} + \frac{1}{v_{gi}}\frac{\partial A_i}{\partial t} = i\kappa A_p A_s^* \exp\left(i\Delta k z\right), \tag{A1a}$$

$$\frac{\partial A_s}{\partial z} + \frac{1}{v_{gs}}\frac{\partial A_s}{\partial t} = i\kappa A_p A_i^* \exp\left(i\Delta k z\right), \tag{A1b}$$

$$\frac{\partial A_p}{\partial z} + \frac{1}{v_{gp}}\frac{\partial A_p}{\partial t} = i\kappa A_i A_s \exp\left(-i\Delta k z\right), \tag{A1c}$$

Considering monochromatic continuous waves and assuming that the pump wave is not depleted, i.e. $A_p\left(z\right) = A_{p0}$, the latter coupled equations reduce to

$$\frac{\mathrm{d}A_i}{\mathrm{d}z} = i\kappa A_{p0} A_s^* \exp\left(i\Delta k z\right), \tag{A2a}$$

$$\frac{\mathrm{d}A_s}{\mathrm{d}z} = i\kappa A_{p0} A_i^* \exp\left(i\Delta k z\right). \tag{A2b}$$

When there is no input for the idler wave, i.e. $A_i\left(0\right) = 0$, the gain for the signal intensity after a single pass in the FWOPA, $\left|A_s\left(L\right)\right|^2 / \left|A_s\left(0\right)\right|^2 = 1 + G_{\mathrm{FWOPA}}$, can be determined by solving (A2a) and (A2b) to be

$$G_{\mathrm{FWOPA}} = \frac{4\kappa^2 \left|A_{p0}\right|^2}{4\kappa^2 \left|A_{p0}\right|^2 - \Delta k^2} \sinh^2\left[\left(4\kappa^2 \left|A_{p0}\right|^2 - \Delta k^2\right)^{1/2} L/2\right], \tag{A3}$$

A.2. SROPO build-up time

Let us consider a SROPO characterized by a cavity round-trip time, τ_{cav}, and a coupler reflectivity, R, while the other cavity loss are negligible. Considering that the pump is not depleted during the oscillation build-up time, the intracavity signal intensity temporal evolution can approximated by

$$I_s\left(t\right) = I_s\left(0\right)\left[R\cosh^2\left(\kappa\left|A_{p0}\right| L\right)\right]^{t/\tau_{\mathrm{cav}}}, \tag{A4}$$

where perfect phase matching was assumed in (A3). The above expression can be rewritten

$$I_s\left(t\right) = I_s\left(0\right)\exp\left(t/\tau_{\mathrm{SROPO}}\right), \tag{A5}$$

with

$$\tau_{\mathrm{SROPO}} = \frac{\tau_{\mathrm{cav}}}{\ln\left(R\right) + 2\ln\left\{\cosh\left[\cosh^{-1}\left(1/\sqrt{R}\right) u_{p0}/u_{\mathrm{th,SROPO}}^{\mathrm{CW}}\right]\right\}} \tag{A6}$$

and

$$u_{\mathrm{th,SROPO}}^{\mathrm{CW}} = \frac{1}{\kappa L}\cosh^{-1}\left(\frac{1}{\sqrt{R}}\right) \tag{A7}$$

A.3. Cavity-enhanced FWOPA gain spectrum

We now consider the CE-FWOPA (or sub-threshold SROPO). Assuming that the signal frequency is a cavity eigenfrequency, the gain of the CE-FWOPA can be written

$$G_{\mathrm{CE-FWOPA}} = \frac{(1-R)\, G_{\mathrm{FWOPA}}}{\left[1-\sqrt{R\,(1+G_{\mathrm{FWOPA}})}\right]^2}. \tag{A8}$$

such as the signal intensity incident on the cavity, I_s^{in}, is related to the output signal intensity, I_s^{out}, by $I_s^{\mathrm{out}}/I_s^{\mathrm{in}} = 1 + G_{\mathrm{CE-FWOPA}}$. Inserting (A3) in (A8), one obtains the following expression:

$$\begin{aligned} G_{\mathrm{CE-FWOPA}} = {} & (1-R)\, 4\kappa^2 \left|A_{p0}\right|^2 \\ & \times \sinh^2\left[\left(4\kappa^2\left|A_{p0}\right|^2 - \Delta k^2\right)^{1/2} L/2\right] \Bigg/ \Bigg[\left(4\kappa^2\left|A_{p0}\right|^2 - \Delta k^2\right)^{1/2} \\ & - \sqrt{R}\left\{4\kappa^2\left|A_{p0}\right|^2 \cosh^2\left[\left(4\kappa^2\left|A_{p0}\right|^2 - \Delta k^2\right)^{1/2} L/2\right] - \Delta k^2\right\}^{1/2}\Bigg]^2. \end{aligned} \tag{A9}$$

Funding. European Union's Horizon 2020 research and innovation program under grant agreement No. 821868 (project LEMON). French Agence Nationale pour la Recherche (ANR) under grant No. ANR-16-CE01-0009 (project WaVIL), and as part of the "Investissements d'Avenir" program (ANR-10-LABX-0039-PALM, Labex PALM) (project SACLAD)

Acknowledgments. The authors are grateful to Prof. Valdas Pasiskevicius for critical reading of the manuscript.

Disclosures. The authors declare no conflicts of interest.

Data Availability. Data underlying the results presented in this paper are not publicly available at this time but may be obtained from the authors upon reasonable request.

References

1. S. E. Harris, "Proposed backward wave oscillation in the infrared," Appl. Phys. Lett. **9**, 114–116 (1966).
2. C. Canalias and V. Pasiskevicius, "Mirrorless optical parametric oscillator," Nat. Photon **1**, 459–462 (2007).
3. G. Strömqvist, V. Pasiskevicius, C. Canalias, and C. Montes, "Coherent phase-modulation transfer in counterpropagating parametric down-conversion," Phys. Rev. A **84**, 023825 (2011).
4. G. Strömqvist, V. Pasiskevicius, C. Canalias, P. Aschieri, A. Picozzi, and C. Montes, "Temporal coherence in mirrorless optical parametric oscillators," J. Opt. Soc. Am. B **29**, 1194 (2012).
5. A.-L. Viotti, F. Laurell, A. Zukauskas, C. Canalias, and V. Pasiskevicius, "Coherent phase transfer and pulse compression at 14 μm in a backward-wave OPO," Opt. Lett. **44**, 3066 (2019).
6. A.-l. Viotti, A. Zukauskas, C. Canalias, F. Laurell, and V. Pasiskevicius, "Narrowband, tunable, infrared radiation by parametric amplification of a chirped backward-wave OPO signal," Opt. Express **27**, 10602 (2019).
7. J. G. Meadors, "Steady-state theory of backward-traveling-wave parametric interactions," J. Appl. Phys. **40**, 2510–2512 (1969).
8. H. Hsu and C. Yu, "Parametric amplification and oscillation in nonlinear backward scattering," Appl. Phys. Lett. **22**, 41–43 (1973).
9. C. Yu and H. Hsu, "The reflection coefficient in stimulated parametric backscattering," J. Appl. Phys. **48**, 2089–2090 (1977).
10. Y. Ding and J. Khurgin, "Backward optical parametric oscillators and amplifiers," IEEE J. Quantum Electron. **32**, 1574–1582 (1996).
11. R. S. Coetzee, A. Zukauskas, C. Canalias, and V. Pasiskevicius, "Low-threshold, mid-infrared backward-wave parametric oscillator with periodically poled Rb:KTP," APL Photonics **3**, 071302 (2018).
12. S. Brosnan and R. Byer, "Optical parametric oscillator threshold and linewidth studies," IEEE J. Quantum Electron. **15**, 415–431 (1979).
13. C. E. Minor and R. S. Cudney, "Mirrorless optical parametric oscillation in bulk PPLN and PPLT: a feasibility study," Appl. Phys. B **123**, 38 (2017).

14. E. Rosencher and C. Fabre, "Oscillation characteristics of continuous-wave optical parametric oscillators: beyond the mean-field approximation," J. Opt. Soc. Am. B **19**, 1107 (2002).
15. A. Godard and E. Rosencher, "Energy yield of pulsed optical parametric oscillators: a rate-equation analysis," IEEE J. Quantum Electron. **40**, 784–790 (2004).
16. G. Aoust, A. Godard, M. Raybaut, J.-B. Dherbecourt, G. Canat, and M. Lefebvre, "Pump duration optimization for optical parametric oscillators," J. Opt. Soc. Am. B **31**, 3113 (2014).
17. G. Aoust, A. Godard, M. Raybaut, O. Wang, J.-M. Melkonian, and M. Lefebvre, "Optimal pump pulse shapes for optical parametric oscillators," J. Opt. Soc. Am. B **33**, 842 (2016).
18. A. V. Smith, R. J. Gehr, and M. S. Bowers, "Numerical models of broad-bandwidth nanosecond optical parametric oscillators," J. Opt. Soc. Am. B **16**, 609 (1999).
19. M. Abramowitz and I. Stegun, *Handbook of Mathematical Functions* (Dover, New York, 1970).
20. Z. Sacks, O. Gayer, E. Tal, and A. Arie, "Improving the efficiency of an optical parametric oscillator by tailoring the pump pulse shape," Opt. Express **18**, 12669 (2010).
21. D. S. Chemla, E. Batifol, R. L. Byer, and R. L. Herbst, "Optical backward mixing in sodium nitrite," Opt. Commun. **11**, 57–61 (1974).
22. A. V. Smith, "Bandwidth and group-velocity effects in nanosecond optical parametric amplifiers and oscillators," J. Opt. Soc. Am. B **22**, 1953 (2005).
23. R. L. Sutherland, *Handbook of nonlinear optics* (CRC Press, 2003).